

## Synthesis, characterization and computational investigation of 5-chloro-2-(5-(2-methyl-1H-benzimidazol-5-yl)-1,3,4-oxadiazol-2-yl)aniline: DFT, parr indices, ADMET, molecular docking and molecular dynamics

Assiya Atif<sup>a\*</sup>, Bendaoud Ahmed<sup>b</sup>, Houssine Ait Sir<sup>a</sup>, Salah Mohammed<sup>b</sup> and Zeroual Abdellah<sup>b</sup>

<sup>a</sup>Bioorganic Chemistry Team, Laboratory of Bioorganic Chemistry, Faculty of Sciences, Chouaib Doukkali University, 24000 El Jadida, Morocco

<sup>b</sup>Molecular Modeling and Spectroscopy Research Team, Faculty of Sciences, Chouaib Doukkali University, 24000 El Jadida, Morocco

### CHRONICLE

#### Article history:

Received April 14, 2025

Received in revised form

June 15, 2025

Accepted October 31, 2025

Available online

October 31, 2025

#### Keywords:

1,3,4-oxadiazole

Synthesis

Characterization

DFT

ESP

Fukui indices

ADME/Tox

Molecular docking

Molecular Dynamics

### ABSTRACT

This study presents the synthesis and characterization of the compound 5-chloro-2-(5-(2-methyl-1H-benzimidazol-5-yl)-1,3,4-oxadiazol-2-yl)aniline, by <sup>1</sup>H NMR, <sup>13</sup>C NMR, FTIR-ATR infrared spectroscopy and mass spectrometry. The theoretical investigation was evaluated using density functional theory (DFT), electrostatic surface potential (ESP) analysis as well as Fukui indices, ADME/Tox properties, molecular docking and Molecular Dynamics studies of this molecule.

© 2026 by the authors; licensee Growing Science, Canada.

## 1. Introduction

Heterocyclic compounds are cyclic compounds that have at least two distinct elements in their ring<sup>1-12</sup>. They are the equivalent of homocyclic compounds, which have a ring consisting exclusively of atoms of the same element. Heterocyclic compounds have one or more atoms of an element other than carbon in their ring structure, such as sulfur, oxygen or nitrogen. Atoms that substitute for carbon atoms in the ring and are not carbon are called heteroatoms. Oxadiazole and its derivatives occupy a significant place in pharmaceutical chemistry, facilitating the synthesis of a multitude of heterocyclic compounds incorporating oxadiazole, with diverse biological activities<sup>13-19</sup>. Oxadiazole is a five-membered heterocyclic compound that contains two carbon atoms as well as three heterogeneous atoms (N, O). Oxadiazole is considered an extremely useful compound, frequently used in research as a constituent of complex chemical compounds, including drugs. Four isomers of oxadiazole can be distinguished depending on the position of the nitrogen atom in the ring: 1,2,3-oxadiazole, 1,2,4-oxadiazole, 1,2,5-oxadiazole and 1,3,4-oxadiazole. Among this category, 1,3,4-oxadiazoles have been shown to be the most biologically efficient<sup>20-25</sup>.

A large number of 1,3,4-oxadiazole derivatives exhibit diverse biological activities, including antibacterial<sup>26-27</sup>, antimycobacterial<sup>28</sup>, antifungal<sup>29,30</sup>, anti-inflammatory<sup>31,32</sup>, analgesic<sup>33</sup> and anticonvulsant<sup>34,35</sup>.

\* Corresponding author

E-mail address [assia.atif@gmail.com](mailto:assia.atif@gmail.com) (A. Atif)

© 2026 by the authors; licensee Growing Science, Canada

doi: 10.5267/j.ccl.2025.10.006

The structure of oxadiazole is also referred to as azoximes, Diazoxol, furadiazole, biozol, furoxanes and oxybiazole. Due to its resonance energy of approximately 167.4 kJ/mol, the oxadiazole ring exhibits thermostability, which is enhanced by substitution at position 2<sup>36</sup>.

Oxadiazole and its isomers, due to their ability to establish hydrogen bonds with the target site, are attracting great interest in the fields of chemistry, medicine and pharmacy for the development of new drugs. In addition, this molecular cycle is found in a variety of major drugs, such as furamizole which has strong antibacterial action, tiadazosin used as an antihypertensive, zibotentan, an FDA-approved cancer drug. Nesapidil with antiarrhythmic activity and Setileuton which a potent and selective inhibitor of the 5-lipoxygenase (5-LO) enzyme, which plays a key role in producing leukotrienes<sup>37,38</sup>. (Fig 1.)

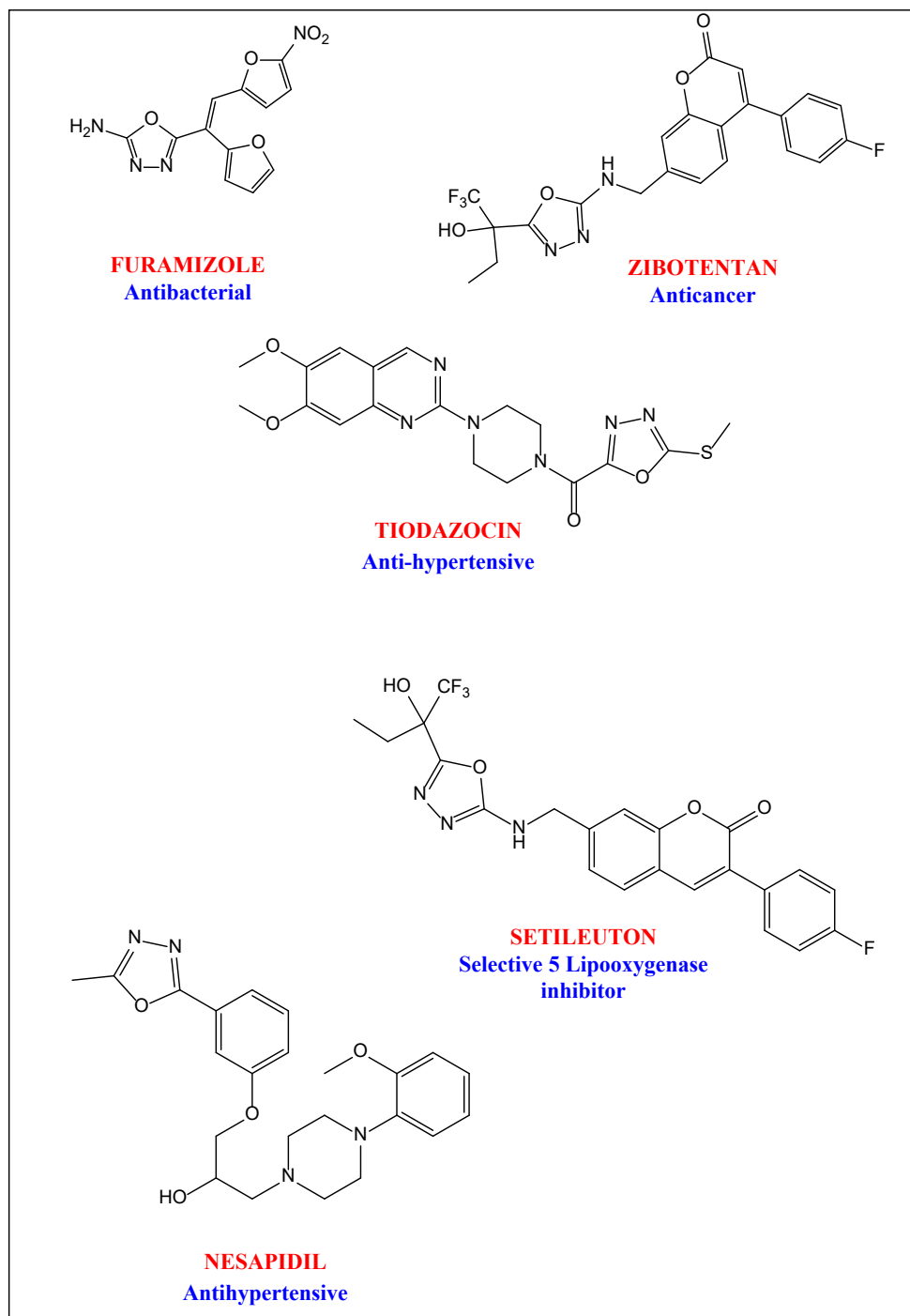


**Fig 1.** Structure of furamizole, tiadazosin, zibotentan, Nesapidil and Setileuton<sup>30,31</sup>.

The compound 5-chloro-2-(5-(2-methyl-1H-benzo[d]imidazol-5-yl)-1,3,4-oxadiazol-2-yl)aniline (BOA) was experimentally synthesized as part of a project aimed at evaluating its biological and anticorrosive properties. Its hybrid structure, incorporating conjugated heteroaromatic moieties, confers promising pharmacological and physicochemical potential, thereby warranting a comprehensive investigation into its mechanisms of action. The adopted methodology

integrates synthetic experimentation with theoretical modeling, with the objective of gaining deeper insights into the compound's reactivity, molecular interactions and behavior on metallic surfaces.

## 2. Materials and Methods

### 2.1. Reagents and instruments

All reagents and solvents were obtained from Sigma Aldrich and used as received. Reaction progress is monitored by thin-layer chromatography (TLC) on aluminum sheets coated with Merck 60 F254 silica gel (thickness 0.2 nm). Revelation is carried out under a UV-Visible lamp (at 254 and 365 nm). The melting points of the synthesized compounds were determined using a Köfler bench in degrees Celsius. FTIR spectra were recorded on a SHIMADZU FT-IR 8400S spectrometer with a Smart iTR accessory and attenuated with total reflection crystal diamond (ATR) in the range (500-4000  $\text{cm}^{-1}$ ). Spectra were recorded on a Fourier transform JNM-ECZ500/S1 FT NMR SYSTEM (JEOL) (500 MHz for proton and 125 MHz for carbon 13) at the Centre National pour la Recherche Scientifique et Technique (CNRST) in Rabat. Spectra are referenced to the solvent in which they were made ( $^1\text{H}$  NMR: DMSO- $d_6$  = 2.5 ppm and  $^{13}\text{C}$  NMR: DMSO- $d_6$  = 39.7 ppm). High-resolution mass spectrometry is performed on an Ultimate 3000-Exactive plus THERMO quadrupole-Orbitrap instrument, equipped with a collision cell from the Centre National pour la Recherche Scientifique et Technique (CNRST) in Rabat.

### 2.2. Calculation methodology

The theoretical investigation begins with an analysis of the electronic structure of BOA using Density Functional Theory (DFT), implemented via the Gaussian 09<sup>39</sup> software package with the B3LYP/6-311G(d,p) basis set. The B3LYP/6-311G(d,p) level of theory was selected for this study because of its proven reliability in describing the electronic and structural properties of organic and coordination compounds. The hybrid B3LYP functional combines the Lee–Yang–Parr correlation functional with a fraction of exact Hartree–Fock exchange, providing accurate predictions of orbital energies, optimized geometries and molecular reactivity indices<sup>40,41</sup>. The 6-311G(d,p) basis set, a triple- $\zeta$  valence basis augmented with polarization functions, enhances the flexibility of atomic orbitals and the accuracy of electron density distribution, especially around heteroatoms<sup>42</sup>. This level of theory thus offers an optimal balance between computational cost and accuracy, making it particularly suitable for reactivity studies based on Density Functional Theory (DFT)<sup>43</sup>. This step enables the geometric optimization of the molecule and the calculation of key reactivity descriptors, including HOMO–LUMO energies, chemical hardness and softness and chemical potential. Electrostatic potential surface (ESP) mapping is complemented by Electron Localization Function (ELF)<sup>44</sup> and Non-Covalent Interaction (NCI) analyses<sup>45</sup>, to identify reactive sites and characterize intra- and intermolecular interactions. Furthermore, Fukui indices are computed to pinpoint the most electrophilic and nucleophilic centers within the molecule. From a pharmacological standpoint, the compound's ADME/Tox properties are evaluated using the SwissADME platform, focusing particularly on AMES toxicity<sup>46</sup>, oral bioavailability and membrane permeability, in order to assess its potential as a therapeutic agent. In a subsequent phase, molecular docking studies are conducted to explore the interaction of BOA with several bacterial protein targets: *Escherichia coli* (PDB ID: 1KZN), *Salmonella enterica* (2XF4), *Staphylococcus aureus* (5TW8) and *Pseudomonas aeruginosa* (4P74). These studies serve to evaluate the ligand's binding affinity to each protein and to characterize the nature of stabilizing interactions at their active sites. Finally, to assess the efficacy of BOA as a corrosion inhibitor, molecular dynamics (MD) simulations are performed. These simulations aim to model the adsorption behavior of the compound on a mild steel surface, thereby predicting the stability of the BOA–iron complex and providing atomic-level insights into its inhibition mechanism.

### 2.3. Synthesis

#### 2.3.1. Synthesis of 2-methyl-1H-benzimidazole-carboxylic acid (**2**)

The reaction of 3,4-diaminobenzoic acid (**1**) (40 mmol) with glacial acetic acid (60 mmol) in concentrated hydrochloric acid (30 ml). The reaction mixture was heated at reflux for a period of six hours. After cooling, a 25% ammonia solution was added to the reaction medium in order to restore its pH to 4. The precipitate obtained was subjected to filtration and recrystallization from ethanol, appearing in the form of a brownish powder<sup>47-49</sup>. Solid brown; 85%; > 300°C,  $^1\text{H}$  NMR(500MHz,DMSO- $d_6$ ppm): 2.56(s,3H,CH<sub>3</sub>), 7.16(d,J=5Hz,1H,CHar), 7.56(s,1H,CHar), 7.87(d,J=5Hz,1H,CHar), 10.49(s,1H,NH), 11.00(s,1H,OH).  $^{13}\text{C}$  NMR (125MHz,DMSO- $d_6$ , ppm): 160.60(C=O), 155.32(C=N), 146.80(Car), 136.44(Car), 127.83(Car), 127.30(Car), 116.84(Car), 115.10(Car), 19.10(CH<sub>3</sub>). IR-ATR ( $\text{cm}^{-1}$ ): 3225  $\nu\text{N-H}$ , 2962-3218  $\nu\text{O-H}$ , 1712  $\nu\text{C=O}$ , 1625  $\nu\text{C=N}$ . MS(ESI):  $m/z$  = 177 [ $\text{M}+\text{H}$ ]<sup>+</sup> 49.

#### 2.3.2. Synthesis of ethyl 2-methyl-1H-benzimidazole-5-carboxylate (**3**)

The esterification of 2-methyl-1H-benzimidazole-carboxylic acid (**2**) was carried out by reacting 7 mmol of 2-methyl-1H-benzimidazole-carboxylic acid (**2**) with 30 ml of absolute ethanol by adding 8 ml of thionyl chloride at 0 °C, the mixture was refluxed for 24 hours. After the completion of the reaction, a 10% NaHCO<sub>3</sub> solution was used to bring the mixture to

a neutral pH of 7. A buff-colored powder was obtained by filtration and recrystallization of the precipitate from ethanol<sup>49</sup>. Solid *chamois*; 79%; 170-172°C. <sup>1</sup>H NMR(500MHz,DMSO-*d*<sub>6</sub>,ppm): 1.30(t,J=5Hz,3H,CH<sub>3</sub>), 2.56(s,3H,CH<sub>3</sub>), 4.27(q,J=10Hz,2H,CH<sub>2</sub>), 7.24(s,1H,CHar), 7.56(d,J=5Hz,1H,CHar), 8.00(d,J=5Hz,1H,CHar), 11.00(s,1H,NH). <sup>13</sup>C NMR (125MHz,DMSO-*d*<sub>6</sub>, ppm): 162.86(C=O), 156.66(C=N), 148.35(Car), 135.52(Car), 126.44(Car), 124.14(Car), 116.41(Car), 114.79(Car), 69.00(CH<sub>2</sub>), 19.84(CH<sub>3</sub>), 19.10(CH<sub>3</sub>). IR-ATR (cm<sup>-1</sup>): 3321 νN-H, 1718 νC=O, 1632 νC=N. MS(ESI): m/z = 205 [M+H]<sup>+</sup><sup>49</sup>.

### 2.3.3. Synthesis of 2-methyl-1H-benzimidazole-5-carbohydrazide (**4**)

Reaction of ethyl 2-methyl-1H-benzimidazole-5-carboxylate (**3**) (7 mmol) with hydrazine hydrate (10 mL) for 18 hours at room temperature gave 2-methyl-1H-benzimidazole-5-carbohydrazide (**4**). The solid was purified by recrystallization from ethanol, appearing as a brown powder. This was done after concentrating the reaction mixture, followed by several passes of trituration with methanol to remove excess hydrazine hydrate[49]. Solid brown; 80%; 260-262°C. <sup>1</sup>H NMR(500MHz,DMSO-*d*<sub>6</sub>,ppm): 2.74(s,3H,CH<sub>3</sub>), 4.86(s,2H,NH<sub>2</sub>), 7.37(s,1H,CHar), 7.54(d,J=10Hz,1H,CHar), 7.86(d,J=10Hz,1H,CHar), 9.28(s,1H,NH), 10.20(s,1H,NH). <sup>13</sup>C NMR (125MHz,DMSO-*d*<sub>6</sub>, ppm) : 168.22(C=O), 152.67(C=N), 149.33(Car), 135.29(Car), 130.30(Car), 129.85(Car), 117.42(Car), 116.06(Car), 18.91(CH<sub>3</sub>). IR-ATR (cm<sup>-1</sup>): 3331 νN-H, 3212 νN-H, 3101-3192 νNH<sub>2</sub>, 1675 νC=O,1596 νC=N. MS(ESI): m/z = 191 [M+H]<sup>+</sup><sup>49</sup>.

### 2.3.4. Synthesis of 5-chloro-2-(5-(2-methyl-1H-benzimidazol-5-yl)-1,3,4-oxadiazol-2-yl)aniline (**6**)

After dissolving 3 mmol of 2-amino-4-chlorobenzoic acid (**5**) in 15 ml of phosphoryl trichloride, 3 mmol of 2-methyl-1H-benzimidazole-5-carbohydrazide (**4**) was added and heated under reflux for a period of six hours. After the reaction was completed, the resulting precipitate was filtered and recrystallized from ethanol. Then, a 25% ammonia mixture was added until the pH reached 7[50-52]. Solid beige; 89%; 219-221°C. <sup>1</sup>H NMR(500MHz,DMSO-*d*<sub>6</sub>,ppm): 2.55(s,3H,CH<sub>3</sub>), 5.61(s,2H,NH<sub>2</sub>), 7.05(d,J=10Hz,1H,CHar), 7.21(d,J=10Hz,1H,CHar), 7.39(s,1H,CHar), 7.50(d,J=10Hz,1H,CHar), 7.78(d,J=10Hz,1H,CHar), 7.79(s,1H,CHar), 10.24(s,1H,NH). <sup>13</sup>C NMR (125MHz,DMSO-*d*<sub>6</sub>, ppm) : 161.46(C=N), 161.04(C=N), 154.41(C=N), 146.80(Car), 136.44(Car), 135.52(Car), 134.75(Car), 130.08(Car), 128.89(Car), 121.62(Car), 120.80(Car), 117.66(Car), 116.87(Car), 115.65(Car), 114.79(Car), 19.10(CH<sub>3</sub>), IR-ATR (cm<sup>-1</sup>): 3191-3210 νNH<sub>2</sub>, 3095 νN-H, 1659 νC=N, 1291 νC-H. MS(ESI): m/z = 326 [M+H]<sup>+</sup><sup>50,52</sup>.

## 3. Results and Discussion

### 3.1. Synthesis of 5-chloro-2-(5-(2-methyl-1H-benzimidazol-5-yl)-1,3,4-oxadiazol-2-yl)aniline (**6**)

Condensation of 3,4-diaminobenzoic acid (OPDA) with acetic acid in hydrochloric acid medium gave 2-methyl-1H-benzimidazole-5-carboxylic acid (**2**) by Phillips technique in good yield. Next, our working method was to esterify 2-methyl-1H-benzimidazole-5-carboxylic acid (**2**) by activating the carboxylic acid at reflux for 24 hours using ethanol and thionyl chloride. Then, hydrazine hydrate is reacted with ethyl 2-methyl-1H-benzimidazole-5-carboxylate (**3**) for eighteen hours at room temperature to give 2-methyl-1H-benzimidazole-5-carbohydrazide (**4**) in 80% yield<sup>49</sup>. Finally, the condensation of 2-methyl-1H-benzimidazole-5-carbohydrazide (**4**) with 2-amino-4-chlorobenzoic acid (**5**), in the presence of phosphoryl trichloride at reflux allowed us to recover 5-chloro-2-(5-(2-methyl-1H-benzimidazol-5-yl)-1,3,4-oxadiazol-2-yl)aniline (**6**) with a yield of 89%[50-52]. This is a simple one-step method among the various methods for the synthesis of 1,3,4-oxadiazole derivatives<sup>4,5</sup>. (**Scheme 1.**)

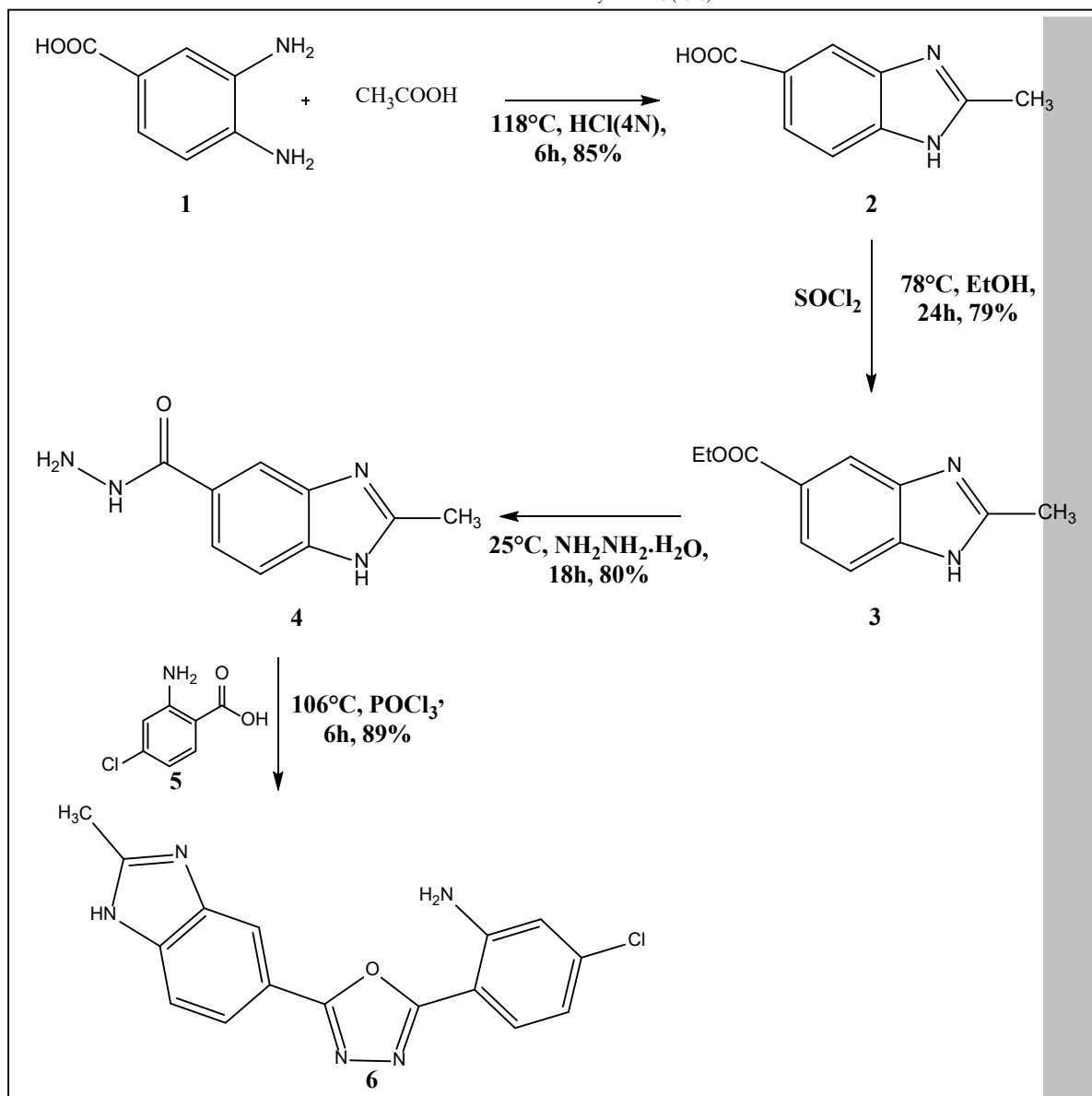
The structure of 5-chloro-2-(5-(2-methyl-1H-benzimidazol-5-yl)-1,3,4-oxadiazol-2-yl)aniline (**6**) was characterized and confirmed using <sup>1</sup>H NMR, <sup>13</sup>C NMR, IR and mass spectrometry spectral data.

<sup>1</sup>H NMR analysis of the isolated compound reveals the presence of a signal at 2.55 ppm corresponding to the methyl proton, a signal at 5.61 relative to the amine proton NH<sub>2</sub>, a deshielded signal at 10.24 due to the N-H proton and clusters between 7.05 and 7.79 ppm corresponding to the aromatic protons.

The <sup>13</sup>C NMR spectrum of the compound reveals a signal at 19.10 ppm attributable to the methyl carbon, signals at 146.80, 136.44, 135.52, 134.75, 130.08, 128.89, 121.62, 120.80, 117.66, 116.87, 115.65 and 114.79 ppm due to the aromatic carbons, as well as three signals at 161.46, 161,04 and 154.41 ppm corresponding to the C=N bonds.

The IR(ATR) spectrum shows an absorption band at 3191-3210 cm<sup>-1</sup> related to NH<sub>2</sub>, a band at 3095 cm<sup>-1</sup> due to N-H, a band at 1659 cm<sup>-1</sup> attributed to the stretching vibration (-C=N) and a band at 1291 cm<sup>-1</sup> corresponding to (-CH) methyl.

Finally, the mass spectrum of our product, taken in (ESI) indicates the presence of a molecular peak at the molecular ion m/z = 326 [M+H]<sup>+</sup>.



**Scheme 1.** Procedure for the synthesis of 5-chloro-2-(5-(2-methyl-1H-benzimidazol-5-yl)-1,3,4-oxadiazol-2-yl)aniline (**6**)

47-52

### 3.2. Theoretical Design

Combined DFT, ADMET, molecular docking, and molecular dynamics studies indicate that the compound BOA exhibits strong electronic reactivity and stable interactions with both metallic surfaces and bacterial proteins. The small HOMO–LUMO energy gap (4.07 eV) and high dipole moment (6.08 D) suggest significant polarity and a high capability to interact with biological and metallic targets. The highly negative adsorption energy (–6020 kcal/mol) confirms stable adsorption on the metal surface, while the docking binding energies (–6.4 to –9.2 kcal/mol) reveal specific interactions with bacterial proteins, notably through hydrogen bonds and  $\pi$ – $\pi$  interactions. Molecular dynamics results, showing a binding energy of 52.4 kcal/mol at 298 K, further confirm efficient and stable adsorption under physiological conditions. Although some pharmacokinetic limitations were identified, such as hepatotoxicity and low solubility, BOA exhibits promising electronic and interaction properties.

#### 3.2.1 Computational Analysis of the Electronic Structure and Adsorption behavior of the BOA Inhibitor on the Fe(110) Surface

The electrostatic potential surface (ESP) analysis reveals a heterogeneous distribution of charges across the BOA molecule, highlighting the presence of electrophilic regions (in red) and nucleophilic regions (in blue/green). These zones correspond to the primary reactive sites likely to interact with surrounding species, particularly with metallic surfaces in the context of corrosion or with cell membranes in the antibacterial context. Frontier molecular orbital (FMO) analysis shows that the highest occupied molecular orbital (HOMO,  $E = -0.05986$  Ha) is predominantly localized around the nitrogen and

oxygen heteroatoms, indicating their key role in donating electrons to the vacant orbitals of the metal (Fe). In contrast, the lowest unoccupied molecular orbital (LUMO,  $E = -0.20958$  Ha) is delocalized over the entire aromatic framework, suggesting a capacity to accept electrons, which promotes a donor–acceptor interaction mechanism with the metallic substrate. The Electron Localization Function (ELF) analysis reveals well-defined basins around nitrogen and oxygen atoms, with high electron populations (e.g.,  $V(N) \approx 23$  e.  $V(O) \approx 4$  e), confirming that these atoms serve as the most active centers for adsorption and complexation. Moreover, the presence of shared basins across the aromatic rings indicates enhanced electronic stability through  $\pi$ -delocalization, which contributes to the compound's inhibitory efficiency. Non-Covalent Interaction (NCI) plots further demonstrate the coexistence of attractive interactions (blue regions, corresponding to hydrogen bonds and electrostatic forces) and weak steric repulsions (red regions). These non-covalent interactions facilitate the stable adsorption of BOA onto the Fe(110) metallic surface, while also strengthening interactions with biological components in bacterial membranes. In summary, the synergy between the high electron density on heteroatoms, the  $\pi$ -electron delocalization and the presence of stabilizing non-covalent interactions endows BOA with a dual functionality: high efficiency as a corrosion inhibitor via surface adsorption on steel and antibacterial potential through its capacity to interact with cellular membranes.

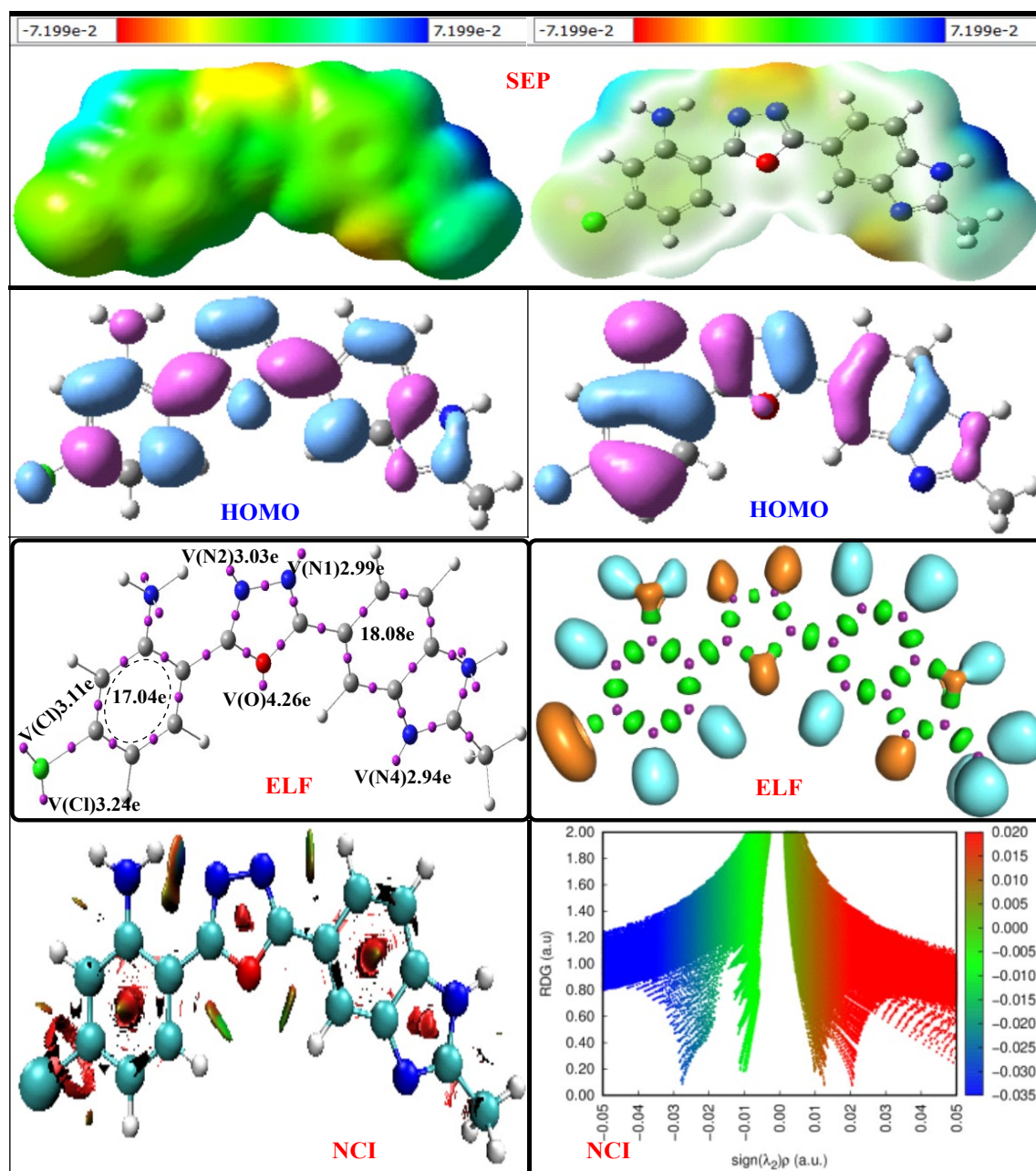


**Fig 2.** electrostatic potential (ESP) isosurface, Highest occupied molecular orbital (HOMO), Lowest unoccupied molecular orbital (LUMO), (A,B) ELF positions basin attractors with ELF localization domains with the greatest relevance for valence basin populations are described at an ELF isosurface value of 0.80, noncovalent interactions (NCI) of BOA inhibitor derived by using DFT/b3lyp/6-311G(d,p) calculations in the aqueous phase

### 3.2.2. DFT calculations for the examination of electronic structure

As part of this theoretical study, the molecular reactivity parameters were evaluated based on the frontier molecular orbital energies namely, the Highest Occupied Molecular Orbital (HOMO) and the Lowest Unoccupied Molecular Orbital (LUMO) obtained through quantum chemical calculations. These quantities form the foundation of the conceptual framework of Density Functional Theory (DFT) and are essential for describing the electronic stability, chemical reactivity and charge transfer propensity of the inhibitor molecule. The energy gap between the frontier orbitals ( $\Delta E = E_{\text{LUMO}} - E_{\text{HOMO}}$ ) reflects the ease of electronic excitation and serves as a fundamental indicator of chemical reactivity. From these values, the chemical hardness ( $\eta = (E_{\text{LUMO}} - E_{\text{HOMO}})/2$ ) and softness ( $\sigma = 1/\eta$ ) were derived, representing the molecule's resistance and susceptibility, respectively, to deformation of its electronic density<sup>53,54</sup>. The electronegativity ( $\chi = -(E_{\text{HOMO}} + E_{\text{LUMO}})/2$ ) was also calculated to characterize the molecule's tendency to attract electrons[55]. In addition, the charge transfer capability between the inhibitor and the metal surface was estimated using the fraction of electron transfer ( $\Delta N$ ), defined according to the following equation<sup>56</sup>:

$$\Delta N = \frac{\chi_{\text{Fe}} - \chi_{\text{inh}}}{2(\eta_{\text{Fe}} - \eta_{\text{inh}})}$$

where  $\chi_{\text{Fe}} = 4.82$  eV and  $\eta_{\text{Fe}} \approx 0$  eV represent the electronegativity and chemical hardness of iron, respectively. A positive value of  $\Delta N$  indicates a net electron transfer from the inhibitor to the metal, suggesting favorable adsorption. Finally, the dipole moment ( $\mu$ ), directly obtained from quantum chemical calculations, was considered as an additional parameter to evaluate the overall polarity of the molecule and its ability to interact with the metallic surface.

**Table 1.** The HOMO and LUMO energy values together with the calculated other related parameters (in eV).

Inhibitor	$E_{\text{HOMO}}$ (eV)	$E_{\text{LUMO}}$ (eV)	$\Delta E$ (eV)	$\eta$ (eV)	$\sigma$ (eV <sup>-1</sup> )	$\chi$	$\Delta N$	$\mu$ (Debye)
BOA	-5.70	-1.63	4.07	2.04	0.49	7.33	-2.56	6.09

The study of BOA's molecular reactivity parameters, derived from frontier molecular orbital (HOMO–LUMO) theory and other quantum descriptors, provides valuable insight into its potential efficiency as a corrosion inhibitor for steel. The relatively high energy of the HOMO ( $-0.20958$  eV) suggests a strong ability of the molecule to donate electrons to the metal surface, while the low energy of the LUMO ( $-0.05986$  eV) indicates a favorable tendency to accept electrons. The small energy gap between HOMO and LUMO ( $\Delta E = 4.07409$  eV) reflects suitable chemical reactivity, compatible with effective interaction between the molecule and the metal substrate. The calculated electronic softness ( $\sigma = 0.49091$  eV<sup>-1</sup>) and high electronegativity ( $\chi = 7.33184$ ) further support this interaction capacity, promoting the adsorption of BOA onto the steel surface. Moreover, the negative value of the electron transfer fraction ( $\Delta N = -2.55386$ ) indicates a net flow of electrons from the metal to the molecule, characteristic of a chemisorption mechanism likely to form a protective film. Finally the high dipole moment ( $\mu = 6.089576$  Debye) suggests significant polarity, which enhances adsorption in aqueous environments. These results confirm that BOA possesses the necessary electronic properties to effectively inhibit corrosion by forming a protective barrier on steel and limiting the access of corrosive agents to the metal surface.

### 3.2.3. Local reactivity indexes

Parr indices are a reliable tool for evaluating local nucleophilicity and electrophilicity in molecules. They are based on the analysis of atomic spin density (ASD) of radical species (radical cation and radical anion) within the unrestricted formalism (B3LYP). The indices are defined as follows<sup>57</sup>:

$$P_k^- = \rho_s^{\text{rc}}(k) \text{ for electrophilic attacks}$$

$$P_k^+ = \rho_s^{\text{ra}}(k) \text{ for nucleophilic attacks}$$

where  $\rho_s^{\text{rc}}(k)$  corresponds to the atomic spin density of the radical cation and  $\rho_s^{\text{ra}}(k)$  to that of the radical anion at a given atom  $k$ . In this study, the Parr functions  $P_k^+$  and  $P_k^-$  were calculated at the B3LYP/6-311G(d,p) level of theory to identify the most reactive sites for nucleophilic and electrophilic attacks on the studied molecule.

The local Parr functions  $P_k^+$  and  $P_k^-$ , calculated at the B3LYP/6-311G(d,p) level of theory, provide an accurate mapping of the preferential reactive sites within the BOA molecule. Regions displaying high  $P_k^-$  values correspond to areas with a strong tendency to donate electron density, thereby exhibiting a pronounced nucleophilic character and favoring interactions with electrophilic centers on the metallic surface. Conversely, sites characterized by elevated  $P_k^+$  values have an enhanced capacity to accept electron density, revealing an electrophilic character that facilitates back-donation from the metal's d-orbitals. In the present study, the Parr-function analysis highlights several carbon atoms particularly C4, C1, C17, C21 and C10 as the most reactive centers, simultaneously showing significant  $P_k^-$  and  $P_k^+$  magnitudes. This duality suggests that these sites participate in a bidirectional electron exchange with the metal surface, combining donation from the inhibitor to the

metal with back-donation from the metal to the molecule. Such a donor–acceptor synergy underlies the formation of a strong, partially covalent adsorption bond on Fe<sup>2+</sup>/Fe<sup>3+</sup> surfaces, leading to the stabilization of a protective molecular film. Although the nitrogen and oxygen atoms (notably N2, N3, N20, and O5) display comparatively lower Parr-function values, their lone pairs can nonetheless contribute to the adsorption process through electrostatic interactions or localized coordination upon metal approach. When considered alongside the ELF and NCI analyses, the Parr-function results indicate that the carbon-centered conjugated framework governs the primary electronic anchoring, while the heteroatoms reinforce the overall stabilization. Collectively, these findings confirm BOA’s strong affinity for the metal surface and its capacity to form a robust protective layer, consistent with its efficiency as a corrosion inhibitor.

**Table 2.** Local Parr reactivity descriptors ( $P_k^+$  and  $P_k^-$ ) computed at the B3LYP/6-311G(d,p) level of theory.

Site	$P_k^+$	$P_k^-$
1 C	0.41	0.31
2 N	-0.19	-0.27
3 N	-0.29	-0.36
4 C	0.52	0.43
5 O	-0.29	-0.33
6 C	-0.21	-0.22
7 C	-0.24	-0.26
8 C	0.17	0.02
9 C	-0.01	-0.01
10 C	0.24	0.18
11 C	0.11	-0.03
12 C	0.11	0.03
13 C	0.13	0.01
14 C	0.22	0.07
15 C	-0.25	-0.26
16 C	0.22	0.05
17 C	0.27	0.24
18 N	0.09	-0.11
19 Cl	0.03	-0.17
20 N	-0.32	-0.361
21 C	0.26	0.22
22 N	-0.19	-0.25
23 C	0.20	0.07

## ADMET prediction

**Table 3.** ADMET prediction for all the synthesized compound (BOA).

Properties	Compound
	BOA
Water solubility	-3.015
Intestinal absorption (human) %	98.218
VDss (human) (log L/kg)	-0.025
BBB permeability (log BB)	-1.189
CNS permeability (log PS)	-2.091
CYP2D6 substrate	No
CYP3A4 substrate	No
CYP1A2 inhibitor	Yes
CYP2C19 inhibitor	Yes
CYP2C9 inhibitor	Yes
CYP2D6 inhibitor	No
CYP3A4 inhibitor	Yes
Total Clearance (log ml/min/kg)	0.732
AMES toxicity	Yes
hERG I inhibitor	No
hERG II inhibitor	Yes
Hepatotoxicity	Yes
Skin Sensitisation	No

The analysis of the ADMET parameters of the compound BOA highlights a pharmacokinetic profile that is both promising and restrictive. Despite limited aqueous solubility ( $\log S = -3.015$ ), the compound shows a particularly high intestinal absorption (98.21%), indicating favorable oral bioavailability. The volume of distribution ( $\log VD_{ss} = -0.025$  log L/kg) points to limited tissue distribution, with the molecule remaining mostly confined to the plasma compartment. Additionally, brain permeability values ( $\log BB = -1.189$ ;  $\log PS = -2.091$ ) confirm an inability to effectively cross the blood-brain barrier, which limits its potential action within the central nervous system while reducing the risk of neurotoxic effects. From a metabolic standpoint, BOA is not a substrate of the CYP2D6 and CYP3A4 isoenzymes but is distinguished

by significant inhibition of several major isoforms, notably CYP1A2, CYP2C19, CYP2C9 and CYP3A4. This inhibition endows the compound with a high potential for drug interactions that could alter the metabolism of co-administered substances. Elimination is characterized by moderate clearance (0.732 log ml/min/kg), suggesting relatively slow excretion and prolonged persistence in the body. Toxicologically, the absence of mutagenicity (negative AMES test) and skin sensitization is a positive aspect. However, the detection of hepatotoxicity and inhibition of the hERG II channel reveal potential risks of liver and cardiac toxicity. In summary, although BOA presents an absorption and distribution profile compatible with promising pharmacological activity, its metabolic properties and toxic potential remain significant obstacles to therapeutic development. Overall, despite certain metabolic and toxicological limitations the pharmacokinetic properties of BOA suggest sufficient bioavailability and potential efficacy against the targeted pathogens, including *E. coli*, *P. aeruginosa*, *S. aureus* and *S. enterica*.

### Molecular docking

The compound BOA, an oxadiazole-based derivative, is recognized for its promising pharmacological properties, particularly its potential antibacterial activity. In this study, molecular docking simulations were performed to evaluate the interactions between the BOA ligand and selected bacterial target proteins<sup>58</sup> and to compare its binding performance with that of a reference antibiotic drug, ciprofloxacin<sup>59,60</sup>. This comparison aimed to assess the relative inhibitory potential and binding selectivity of BOA against key pathogenic bacterial targets. The three-dimensional crystal structures of the bacterial target proteins were retrieved from the Protein Data Bank (PDB) in .pdb format<sup>61</sup>. The selected targets included *Escherichia coli* (PDB ID: 1KZN), *Salmonella enterica* (PDB ID: 2XF4), *Staphylococcus aureus* (PDB ID: 5TW8) and *Pseudomonas aeruginosa* (PDB ID: 4P74). Protein preparation was performed using Discovery Studio<sup>62</sup>, which allowed the removal of crystallographic water molecules, co-crystallized ligands and other non-essential heteroatoms or ions that might interfere with docking accuracy. The active binding sites of each protein were defined using UCSF Chimera<sup>63</sup> by generating a three-dimensional grid box centered on the catalytic pocket of each enzyme, ensuring precise delimitation of the ligand–protein interaction region<sup>64</sup>. To validate the reliability of the docking protocol, a redocking procedure of the BOA ligand was carried out for each protein target<sup>65</sup>. The grid box parameters used are summarized as follows:

**Table 4.** Redocking results of the BOA ligand: grid box parameters and RMSD values for each target protein.

Native Ligand	PDB ID	Number Grid Point			Coordinate Grid Point			Spacing Grid Point	RMSD
		X	Y	Z	X	Y	Z		
BOA	1KZN	9.51	14.38	15.12	18.31	30.75	36.77	0.375	0.9992
	2XF4	9.83	3.77	7.81	-25.98	32.01	-4.49	0.375	1.9095
	5TW8	58	60	58	20.51	-62.21	36.23	0.375	3.8208
	4P74	13.06	6.99	9.95	44.79	-21.89	23.31	0.375	1.2355

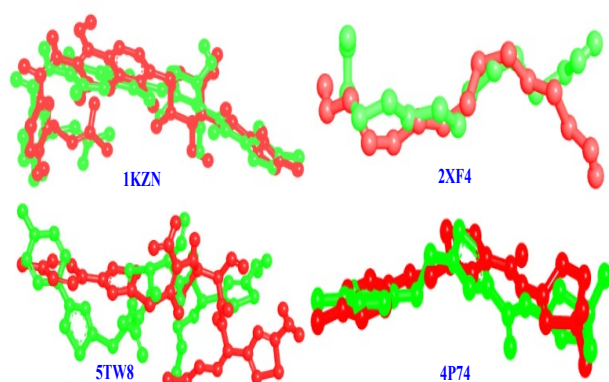


**Fig. 3.** Overlap of Natural Ligand (Green) and Post-Redocking Ligand (red).

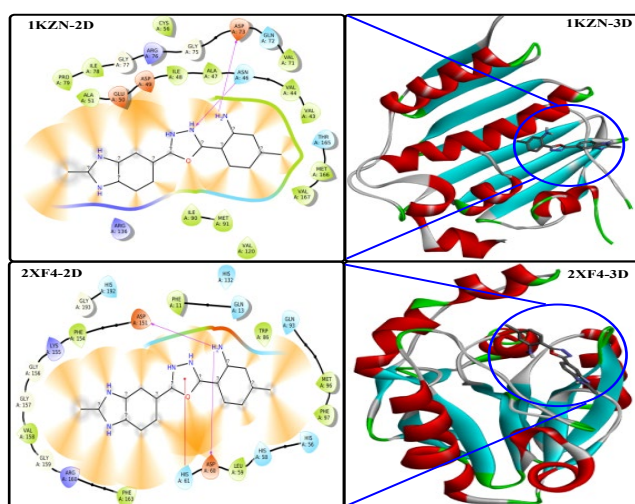


**Fig 4.** Non-covalent interaction network in 2XF4 protein of *S. enterica* and 1KZN protein of *E. coli* and. 2D and 3D ligand complex.

The molecular docking analysis of the BOA inhibitor against various bacterial target proteins revealed notable differences in binding energies, interaction profiles and complex stability, demonstrating an overall higher binding affinity compared to the reference compound, ciprofloxacin. For the *Escherichia coli* protein (PDB ID: 1KZN), BOA exhibited a binding energy of  $-8.6$  kcal/mol, which is more favorable than that of ciprofloxacin ( $-7.6$  kcal/mol), indicating a more stable

interaction. The complex is stabilized by several strong hydrogen bonds involving ASN46 (2.30 Å and 2.83 Å) and ASP73 (2.05 Å), reinforced by electrostatic interactions with ARG76 and GLU50 ( $\approx 3.7$ – $4.8$  Å). Additionally, an extensive network of hydrophobic interactions involving VAL43, VAL71, VAL167, ILE78, PRO79, and ALA47 mainly of the Pi-Alkyl and Pi-Sigma types ( $\approx 4.1$ – $5.4$  Å) contributes to the stabilization of the ligand within the catalytic cavity. Three-dimensional visualization confirmed the deep burial of the ligand within the active site, surrounded by  $\alpha$ -helices and  $\beta$ -sheets, reflecting strong structural complementarity. For *Salmonella enterica* (PDB ID: 2XF4), the BOA–protein complex displayed a binding energy of  $-6.4$  kcal/mol, also more favorable than that of ciprofloxacin ( $-3.9$  kcal/mol). The interaction is primarily governed by two strong hydrogen bonds with ASP60 (2.32 Å) and ASP151 (2.21 Å), which provide initial anchoring of the ligand. These are supported by electrostatic contacts with HIS192 and ASP151 ( $\approx 3.7$ – $4.6$  Å), forming Pi-Cation and Pi-Anion interactions. Furthermore, aromatic interactions involving PHE154, PHE163, HIS58 and PHE97 (Pi-Pi stacking and T-shaped,  $\approx 4.0$ – $5.4$  Å) enhance complex stability and explain the higher affinity observed.

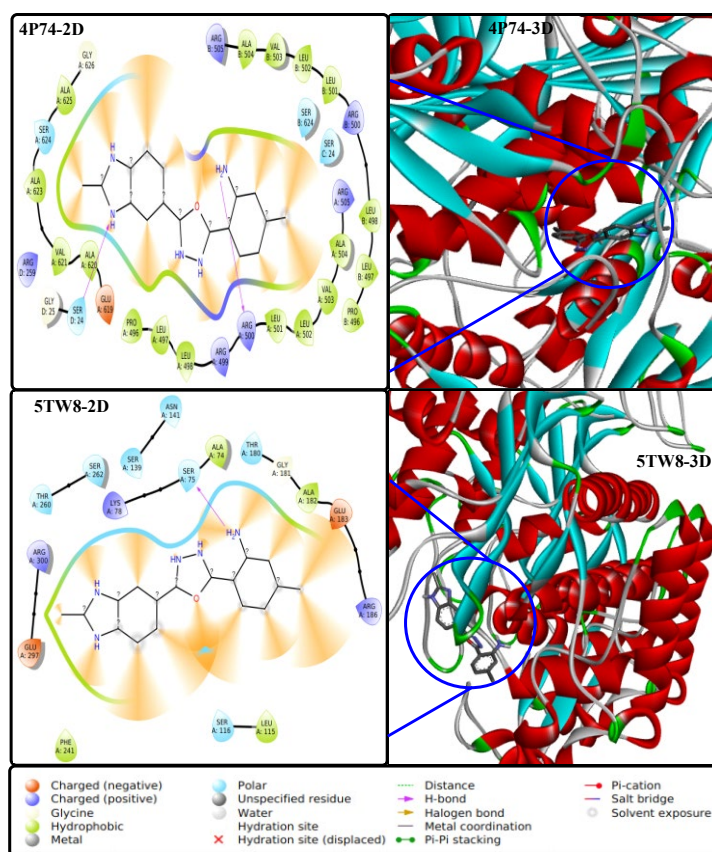


**Fig 5.** Non-covalent interaction network in 4P74 protein of *P. aeruginosa* and 5TW8 protein of *S. aureus*. 2D and 3D Ligand complex.

**Table 5.** Docking scores for all selected compound with their respective target.

Entry	Docking scores Kcal/mol			
	<i>E. coli</i> (PDB ID: 1KZN)	<i>S. enterica</i> (PDB ID: 2XF4)	<i>S. aureus</i> (PDB ID: 5TW8)	<i>P. aeruginosa</i> (PDB ID: 4P74)
<b>BOA</b>	<b>-8.6</b>	<b>-6.4</b>	<b>-9.3</b>	<b>-9.2</b>
<b>Ciprofloxacin</b>	<b>-7.6</b>	<b>-3.9</b>	<b>-8.3</b>	<b>-4.9</b>

These aromatic contacts, absent in the *E. coli* complex, highlight BOA's ability to adapt to different protein environments through diverse interaction modes. In the case of *Staphylococcus aureus* (PDB ID: 5TW8), BOA exhibited the strongest binding affinity among all tested targets, with a docking score of  $-9.3$  kcal/mol, compared to  $-8.3$  kcal/mol

for ciprofloxacin, indicating a more thermodynamically stable complex. The ligand formed four strong hydrogen bonds with SER116, SER139, GLU297 and SER75, with distances ranging from 2.11 to 2.95 Å, reflecting strong polar interactions. Additionally, a specific Pi–Pi stacking interaction with PHE241, combined with strategically positioned hydrophobic contacts, further stabilizes the ligand. The three-dimensional analysis revealed that BOA fits deeply within the catalytic site, adopting a favorable orientation for enzymatic inhibition, confirming optimal structural accommodation and interaction strength. For *Pseudomonas aeruginosa* (PDB ID: 4P74), BOA achieved a binding energy of  $-9.2$  kcal/mol, which is significantly more favorable than that of ciprofloxacin ( $-4.9$  kcal/mol), suggesting a notably stronger binding affinity. In this complex, hydrophobic interactions predominate, mainly involving LEU497, LEU501 and ARG500 through Pi–Alkyl and Alkyl contacts. Although these interactions are less specific than those observed with *S. aureus*, they effectively stabilize the ligand within the catalytic pocket, maintaining a well-oriented and stable complex. Overall, these results clearly indicate that BOA exhibits stronger binding affinities than ciprofloxacin for all four bacterial target proteins, with particularly favorable interactions observed for *Staphylococcus aureus* ( $-9.3$  kcal/mol) and *Pseudomonas aeruginosa* ( $-9.2$  kcal/mol). This enhanced affinity arises from the simultaneous presence of short hydrogen bonds, specific electrostatic and aromatic interactions and a deep insertion of the ligand within the active sites, ensuring optimal conformational stability. The diversity and complementarity of these stabilizing interactions provide BOA with superior binding efficiency compared to the reference antibiotic. Consequently, these findings suggest that BOA is a promising lead compound for the development of new antibacterial agents, exhibiting potential broad-spectrum activity with pronounced selectivity toward *Staphylococcus aureus* and *Pseudomonas aeruginosa*, both of which are clinically significant pathogens.

### 3.2.4. Molecular Dynamics Simulation

Molecular dynamics (MD) simulations were performed using Materials Studio<sup>66,67</sup> software to investigate the adsorption behavior of the BOA inhibitor on an iron metal surface. The crystallographic model of the substrate was constructed by considering the Fe(110) plane, known for its high packing density and thermodynamic stability. A  $7 \times 7$  supercell was generated, followed by the introduction of a 15 Å vacuum region along the c-axis to prevent unwanted periodic interactions<sup>68</sup>. The top layer of the crystal was then removed to create an appropriate simulation box, enabling modeling of the inhibitor adsorption in a mildly acidic aqueous environment. After optimizing the metal surface within Materials Studio, the initial adsorption of the BOA molecule was explored using the Monte Carlo method, which allowed identification of active sites and the most stable conformations on the Fe(110) surface. Based on these results, molecular dynamics<sup>69,70</sup> simulations were subsequently conducted using the COMPASS III force field, known for its reliability in modeling organic and metallic systems. Simulation conditions were set in the NVT ensemble, with a temperature fixed at 298 K and controlled by the Andersen thermostat. Other parameters included a time step of 1.0 fs, a total of 50,000 steps corresponding to a duration of 50 ps. and randomly generated initial velocities. A second simulation was performed under identical conditions but at a higher temperature (398 K) to study the effect of temperature on the stability of the adsorbed complexes. Finally, the interaction energies and binding energies were calculated using the following equation<sup>71</sup>:

$$E_{inter} = E_{complex} - (E_{metal+medium} + E_{inh})$$

$$E_{binding} = -E_{inter}$$

where  $E_{total}$  is the energy of the adsorbed system,  $E_{surface}$  is the energy of the isolated metal surface and  $E_{inhibitor}$  is the energy of the free molecule. These values allowed for the characterization of the thermodynamic stability of the formed complexes and helped relate the adsorption efficiency of the BOA inhibitor to its anticorrosive performance. The liquid phase composed of water (350H<sub>2</sub>O) molecules was added to simulate the effect of solvent since the corrosion takes place in hydrochloric acid solution.

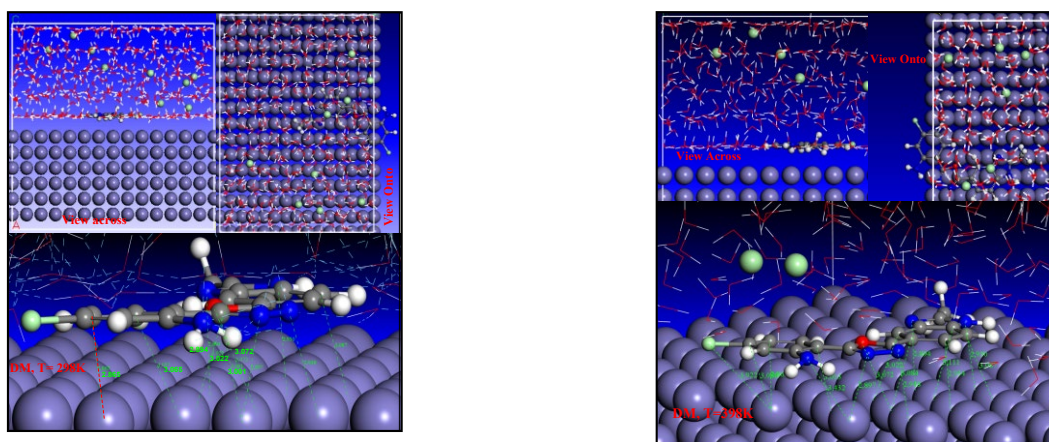


**Fig. 6.** Comparative Adsorption Behavior of an Organic Inhibitor on Fe(110) Surface at 298 K and 398 K: Molecular Dynamics Simulations.

**Table 6.** Monte Carlo simulation results.

Structures	Total energy (Kcal/mol)	Adsorption energy (Kcal/mol)	Rigid adsorption energy (Kcal/mol)	Deformation energy (Kcal/mol)	BOAdft : dEad/dNi (Kcal/mol)	3D Atomistic : dEad/dNi (Kcal/mol)	HCl : dEad/dNi (Kcal/mol)
Fe (1 1 0)	-6.94E+03	-6.02E+03	-6.48E+03	465.5239542	-196.9535152	-15.55669737	-99.5854781

**Table 7.** Molecular Dynamic results.

T(K)	398	298
E <sub>complex</sub> (Kcal/mol)	-70638.3	-71589.2
E <sub>BOA</sub> (Kcal/mol)	-70858.9	-71772.9
E <sub>BOA + H2O+HCl</sub> (Kcal/mol)	236.2	236.2
E <sub>interaction</sub> (Kcal/mol)	-15.4	-52.4
E <sub>binding</sub> (Kcal/mol)	15.4	52.4

In this study, the adsorption of an organic inhibitor on the Fe(110) metal surface was analyzed using Monte Carlo and molecular dynamics methods, employing the Materials Studio software. The Monte Carlo results indicate a highly negative adsorption energy ( $-6020$  kcal/mol), reflecting a stable and spontaneous interaction between the inhibitor molecule and the surface. The relatively low deformation energy (465 kcal/mol) suggests that the molecule easily adapts to the metal surface, supporting the hypothesis of chemisorption-type adsorption. Molecular dynamics simulations conducted at two temperatures (298 K and 398 K) allowed evaluation of the thermal effect on complex stability. At 298 K, the binding energy is high (52.427 kcal/mol), indicating strong adsorption. This interaction is supported by relatively short bond distances between the molecule's atoms and the metal surface, ranging from 2.8 Å to 3.1 Å, confirming strong affinity. Conversely, at 398 K, the binding energy drops to 15 kcal/mol. and the interaction distances increase slightly (some exceeding 3.4 Å), suggesting weakened interactions and a tendency toward desorption. Visual analysis of the configurations shows that the molecule remains well-adhered to the surface at low temperature, whereas at higher temperature, system disorder and partial lifting of the inhibitor are observed. In conclusion, the inhibitor exhibits good adsorption efficiency and protection at ambient temperature, but this efficiency significantly decreases at elevated temperatures, which should be considered for its use in thermally unstable environments.

#### 4. Conclusion

In this work, 5-chloro-2-(5-(2-methyl-1H-benzimidazol-5-yl)-1,3,4-oxadiazol-2-yl)aniline was synthesized and characterized by <sup>1</sup>H NMR, <sup>13</sup>C NMR, FTIR-ATR infrared spectroscopy and mass spectrometry. Electrostatic surface potential (ESP) analysis showed that this molecule has good efficiency as a corrosion inhibitor by adsorption on steel and antibacterial potential thanks to its ability to interact with cell membranes. As well as the molecular reactivity parameters HOMO (Highest Occupied Molecular Orbital) and LUMO (Lowest Unoccupied Molecular Orbital) confirm that BOA has the necessary electronic properties to effectively inhibit corrosion, forming a protective barrier on steel and limiting the access of corrosive agents to its surface. Fukui indices highlight that the local reactivity of BOA is dominated by nitrogen and oxygen atoms, which are the electron donating centers for adsorption on E-24 steel. ADMET parameter analysis of this compound reveals that despite some metabolic and toxicological constraints, these pharmacokinetic properties suggest sufficient bioavailability and potential efficacy against targeted pathogens, including *E. coli*, *P. aeruginosa*, *S. aureus*. and *S. enterica*. The adsorption of this compound on the Fe(110) metal surface was analyzed using Monte Carlo and molecular dynamics methods, which reflects good adsorption and protection efficiency at room temperature. Overall, these results support the bifunctional potential of BOA as a corrosion inhibitor and antibacterial agent. Its favorable electronic characteristics, stable adsorption ability. and specific interactions with bacterial proteins make it a promising candidate for the development of effective antibacterial and anticorrosive inhibitors.

#### Statements & Declarations

##### Funding

The authors declare that no funds, grants or other support were received during the preparation of this manuscript.

##### Competing Interests

The authors have no relevant financial or non-financial interests to disclose.

## Acknowledgements

The authors are grateful to for the research assistance from Bioorganic Chemistry Team, Faculty of Sciences, Chouaib Doukkali University. B.P. 20. 24000 El Jadida. Morocco and Molecular Modeling and Spectroscopy Research Team. Faculty of Science, ChouaibDoukkali University, P.O. Box 20. 24000 El Jadida, Morocco.

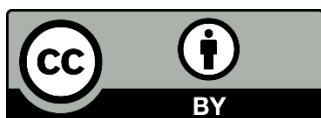
## References

1. Atif A., El Alami A., and Ait Sir H. (2025) Minireview of Synthesis Process of 1.3.4-Thiadiazole Derivatives. *Chem. Afr.*, 8 (7) 1-24.
2. Atif A., and Ait Sir H. (2025) Progress in the Synthesis of Tetrazoles, A Brief Review. *Org. Prep. Proced. Int.*
3. Atif A., and Ait Sir H. (2025) Synthetic Approaches for Oxazole Derivatives: A Review. *Journal of Heterocyclic Chemistry*, 1–26
4. Atif A., Ameer S., and Ait Sir H. (2025) Synthesis. characterization and in silico evaluation of 2.5-bis(2-(trifluoromethyl)-1H-benzimidazol-5-yl)-1.3.4-oxadiazole: Reactivity. ADME/toxicity. and docking against therapeutic targets. *Curr. Chem. Lett.*, 14 (4) 793-804
5. Atif A., El Alami A., Youssoufi F., Jebbari S., and Ait Sir H. (2025). Review of synthesis process of 1.3.4-oxadiazole analogs. *Curr. Chem. Lett.*, 14 (2) 339–364
6. Atif A., Ameer S., and Ait Sir H. (2025) Synthesis. Characterization. and Computational Investigation of 2.5-Bis(2-Methyl-1H-benzimidazol-5-yl)-1.3.4-oxadiazole: Quantum Chemical Analysis. ADME Prediction. Molecular Docking. and MD-Based Corrosion Study for Photonic and Therapeutic Applications. *Curr. Chem. Lett.*
7. Tokmajyan G. G., and Karapetyan L. V. (2025) Methods of synthesis of furan-2 (5 H)-ones. *Chem. Heterocycl. Compd.*, 61 (2025) 73-100.
8. Mitra A. K., and Ghosh A. (2025) Perspective on Biginelli reaction: en route toward the development of biologically and industrially relevant dihydropyrimidone-based frameworks. *Chem. Heterocycl. Compd.*, 61 (2025) 155-187
9. Tokmajyan G. G., and Karapetyan L. V. (2025) Chemical transformations of furan-2 (5 H)-ones. *Chem. Heterocycl. Compd.*, 61 (2025) 101-129.
10. Jasiński R. (2025) Recent progress in the synthesis of nitropyrrolidines via noncatalyzed (3+ 2) cycloaddition reactions of azomethine ylides (microreview). *Chem. Heterocycl. Compd.*, 61 (2025) 240-242.
11. Łapczuk A. (2023) The [3+ 2] cycloaddition reaction as an attractive way for the preparation of nicotine analogs (microreview). *Chem. Heterocycl. Compd.*, 59 (3) 109-111.
12. Sadowski M., and Kula K. (2024) Unexpected course of reaction between (1E, 3E)-1, 4-Dinitro-1, 3-butadiene and n-methyl azomethine ylide—a comprehensive experimental and quantum-chemical study. *Molecules*, 29 (21) 5066-5090.
13. Aggarwal N., Kumar R., Dureja P., and Khurana J. M. (2012) Synthesis of novel nalidixic acid-based 1.3.4-thiadiazole and 1.3.4-oxadiazole derivatives as potent antibacterial agents. *Chem. Biol. Drug Des.*, 79 (4) 384-397.
14. Chawla G., Kumar U., Bawa S., and Kumar J. (2012) Syntheses and evaluation of anti-inflammatory. analgesic and ulcerogenic activities of 1, 3, 4-oxadiazole and 1, 2, 4-triazolo [3, 4-b]-1.3.4-thiadiazole derivatives. *J. Enzyme Inhib. Med. Chem.*, 27 (5) 658-665.
15. Chen C. J., Song B. A., Yang S., Xu G. F., Bhadury P. S., Jin L. H., Hu D. Y., Li Q. Z., Liu F., Xue W., Lu P., and Chen Z. (2007) Synthesis and antifungal activities of 5-(3, 4, 5-trimethoxyphenyl)-2-sulfonyl-1.3.4-thiadiazole and 5-(3,4,5-trimethoxyphenyl)-2-sulfonyl-1, 3, 4-oxadiazole derivatives. *Bioorg. Med. Chem.*, 15 (12) 3981-3989.
16. El-Essawy F. A., El-Sayed W. A., El-Kafrawy S. A., Morshedy A. S., and Abdel-Rahman A. H. (2008) Anti-hepatitis B virus activity of new 1, 2, 4-triazol-2-yl-and 1, 3, 4-oxadiazol-2-yl-2-pyridinone derivatives. *Z. Naturforsch. C.*, 63 (9-10) 667-674.
17. Fan Z., Shi Z., Zhang H., Liu X., Bao L., Ma L., Zuo X., Zheng Q., and Mi N. (2009) Synthesis and biological activity evaluation of 1.2.3-thiadiazole derivatives as potential elicitors with highly systemic acquired resistance. *J. Agric. Food Chem.*, 57 (10) 4279-4286.
18. Garzón A., Granadino-Roldán J. M., Moral M., García G., Fernández-Lienres M. P., Navarro A., Ruiz T. P., and Fernández-Gómez M. (2010) Density functional theory study of the optical and electronic properties of oligomers based on phenyl-ethynyl units linked to triazole, thiadiazole, and oxadiazole rings to be used in molecular electronics. *J. Chem. Phys.*, 132(6) 064901-064913.
19. Gilani S. J., Khan S. A., Alam O., and Siddiqui N. (2011) Synthesis and in vitro antimicrobial evaluation of condensed heterocyclic 6-substituted 1, 2, 4-triazolo-[3, 4-b]-1, 3, 4-thiadiazole and 1.3.4-oxadiazole derivatives of isoniazid. *Acta Pol Pharm.*, 68 (2) 205-211.
20. Küçükgülzel Ş. G., Küçükgülzel I., Tatar E., Rollas S., Şahin F., Güllüce M., Clercq E. D., and Kabasakal L. (2007) Synthesis of some novel heterocyclic compounds derived from diflunisal hydrazide as potential anti-infective and anti-inflammatory agents. *Eur. J. Med. Chem.*, 42 (7) 893-901.
21. Li Y., Geng J., Liu Y., Yu S., and Zhao G. (2013) Thiadiazole—A promising structure in medicinal chemistry. *ChemMedChem.*, 8 (1) 27-41.
22. Mullican M. D., Wilson M. W., Conner D. T., Kostlan C. R., Schrier D. J., and Dyer R. D. (1993) Design of 5-(3, 5-di-tert-butyl-4-hydroxyphenyl)-1, 3, 4-thiadiazoles.-1, 3, 4-oxadiazoles. and-1, 2, 4-triazoles as orally active, nonulcerogenic antiinflammatory agents. *J. Med. Chem.*, 36 (8) 1090-1099.

23. Mylari B. L., Beyer T. A., Scott P. J., Aldinger C. E., Dee M. F., Siegel T. W., and Zembrowski W. J. (1992) Potent orally active aldose reductase inhibitors related to zopolrestat: surrogates for benzothiazole side chain. *J. Med. Chem.*, 35 (3) 457-465.
24. Padmaja A., Muralikrishna A., Rajasekhar C., and Padmavathi V. (2011) Synthesis and antimicrobial activity of pyrrolyl/pyrazolyl arylaminosulfonylmethyl 1. 3. 4-oxadiazoles. 1. 3. 4-thiadiazoles and 1. 2. 4-triazoles. *Chem. Pharm. Bull.*, 59 (12) 1509-1517.
25. Rajak H., Agarawal A., Parmar P., Thakur B. S., Veerasamy R., Sharma P. C., and Kharya M. D. (2011) 2. 5-Disubstituted-1. 3. 4-oxadiazoles/thiadiazole as surface recognition moiety: Design and synthesis of novel hydroxamic acid based histone deacetylase inhibitors. *Bioorg. Med. Chem. Lett.*, 21 (19) 5735-5738.
26. Holla B. S., Gonsalves R., and Shenoy S. (2000) Synthesis and antibacterial studies of a new series of 1. 2-bis (1. 3. 4-oxadiazol-2-yl) ethanes and 1. 2-bis (4-amino-1. 2. 4-triazol-3-yl) ethanes. *Eur. J. Med. Chem.*, 35 (2) 267-271.
27. Şahin G., Palaska E., Ekizoğlu M., and Özalp M. (2002) Synthesis and antimicrobial activity of some 1. 3. 4-oxadiazole derivatives. *Il Farmaco*. 57 (7) 539-542.
28. Macaev F., Rusu G., Pogrebnoi S., Gudima A., Stingaci E., Vlad L., Shvets N., Kandemirli F., Dimoglo A., and Reynolds R. (2005) Synthesis of novel 5-aryl-2-thio-1. 3. 4-oxadiazoles and the study of their structure-anti-mycobacterial activities. *Bioorg. Med. Chem.*, 13 (16) 4842-4850.
29. Tale R. H., Rodge A. H., Keche A. P., Hatnapure G. D., Padole P. R., Gaikwad G. S., and Turkar. S. S. (2011) Synthesis and anti-bacterial. anti-fungal activity of novel 1. 2. 4-oxadiazole. *J. Chem. Pharm. Res.*, 3 (2) 496-505.
30. Zou X. J., Lai L. H., Jin G. Y., and Zhang Z. X. (2002) Synthesis. fungicidal activity. and 3D-QSAR of pyridazinone-substituted 1. 3. 4-oxadiazoles and 1. 3. 4-thiadiazoles. *J. Agric. Food Chem.*, 50 (13) 3757-3760.
31. Burbuliene M. M., Jakubkiene V., Mekuskiene G., Udrenaitė E., Smicius R., and Vainilavicius P. (2004) Synthesis and anti-inflammatory activity of derivatives of 5-[(2-disubstitutedamino-6-methyl-pyrimidin-4-yl)-sulfonylmethyl]-3H-1. 3. 4-oxadiazole-2-thiones. *Il Farmaco*. 59 (10) 767-774.
32. Palaska E., Şahin G., Kelicen P., Durlu N. T., and Altinok G. (2002) Synthesis and anti-inflammatory activity of 1-acylthiosemicarbazides. 1. 3. 4-oxadiazoles. 1. 3. 4-thiadiazoles and 1. 2. 4-triazole-3-thiones. *Il Farmaco*. 57 (2) 101-107.
33. Amir M., and Shikha K. (2004) Synthesis and anti-inflammatory. analgesic. ulcerogenic and lipid peroxidation activities of some new 2-[(2. 6-dichloroanilino) phenyl] acetic acid derivatives. *Eur. J. Med. Chem.*, 39 (6) 535-545.
34. Zarghi A., Tabatabai S. A., Faizi M., Ahadian A., Navabi P., Zanganeh V., and Shafiee A. (2005) Synthesis and anticonvulsant activity of new 2-substituted-5-(2-benzyloxyphenyl)-1. 3. 4-oxadiazoles. *Bioorg. Med. Chem. Lett.* 15 (7) 1863-1865.
35. Almasirad A., Tabatabai S. A., Faizi M., Kebriaeezadeh A., Mehrabi N., Dalvandi A., and Shafiee. A. (2004) Synthesis and anticonvulsant activity of new 2-substituted-5-[2-(2-fluorophenoxy) phenyl]-1. 3. 4-oxadiazoles and 1. 2. 4-triazoles. *Bioorg. Med. Chem. Lett.* 14 (24) 6057-6059.
36. Ainsworth C., and Hackler R. E. (1966) Alkyl-1. 3. 4-oxadiazoles. *J. Org. Chem.*, 31 (10) 3442-3444.
37. Vaidya A., Pathak D., and Shah K. (2021) 1. 3. 4-oxadiazole and its derivatives: A review on recent progress in anticancer activities. *Chem. Biol. Drug Des.* 97 (3) 572-591.
38. Siwach A., and Verma P. K. (2020) Therapeutic potential of oxadiazole or furadiazole containing compounds. *BMC chemistry*. 14 (1) 70-110.
39. VandeVondele J., Krack M., Mohamed F., Parrinello M., Chassaing T., and Hutter J. (2005) Quickstep: Fast and accurate density functional calculations using a mixed Gaussian and plane waves approach. *Comput. Phys. Commun.*, 167 (2) 103-128.
40. Becke A. D. (1993) Density-functional thermochemistry. III. The role of exact exchange. *J. Chem. Phys.*, 98 (7) 5648-5652.
41. Ulufer-bulut S., Kotan G., and Yuksek H. (2021) Theoretical (6-311G (d. p)/3-21G) and Spectroscopic (13C/1H-NMR. FT-IR) Analyses of 3-Propyl-4-[3-(2-Methylbenzoxy)-Benzylidenamino]-4. 5-Dihydro-1H-1. 2. 4-Triazol-5-One Molecule. *eurasia proc. sci. technol. eng. math.* 15 (2021) 42-53.
42. Aytemiz F., Beytur M., and Yuksek H. (2022) Experimental and Gaussian calculations of 3-Ethyl-4-(2-benzenesulfonyloxy)-benzylideneamino-4. 5-dihydro-1H-1. 2. 4-triazol-5-one. *eurasia proc. sci. technol. Eng. Math.*, 20 (2022) 103-111.
43. Krishnan R. B. J. S., Binkley J. S., Seeger R., and Pople J. A. (1980) Self-consistent molecular orbital methods. XX. A basis set for correlated wave functions. *J. Chem. Phys.*, 72 (1) 650-654.
44. Kazachenko A. S., Akman F., Abdelmouli H., Issaoui N., Malyar Y. N., Al-Dossary O., and Wojcik M. J. (2021) Intermolecular hydrogen bonds interactions in water clusters of ammonium sulfamate: FTIR. X-ray diffraction. AIM. DFT. RDG. ELF. NBO analysis. *J. Mol. Liq.*, 342 (2021) 117475-117499.
45. Mazumdar P., Kashyap A., and Choudhury D. (2023) Investigation of hydrogen bonding in small nucleobases using DFT. AIM. NCI and NBO technique. *Comput. Theor. Chem.*, 1226 (2023) 114188-114197.
46. Ojuka P., Kimani N. M., Apollo S., Nyariki J., Ramos R. S., and Santos C. B. (2023) Phytochemistry of plants in the genus *Vepris*: A review and in silico analysis of their ADMET properties. *S. Afr. J. Bot.*, 157 (2023) 106-114.

47. Kaul S., Kumar A., Sain B., and Bhatnagar A. K. (2007) Simple and convenient one-pot synthesis of benzimidazoles and benzoxazoles using N, N-Dimethylchlorosulfitemethaniminium chloride as condensing agent. *Synth. Commun.*, 37 (15) 2457-2460.
48. Phillips M. A. (1928) CCCXVII.—The formation of 2-substituted benzimidazoles. *J. Chem. Soc.*, 2393-2399.
49. Galal S. A., Hegab K. H., Kassab A. S., Rodriguez M. L., Kerwin S. M., El-Khamry A. M. M. A., and El Diwani H. I. (2009) New transition metal ion complexes with benzimidazole-5-carboxylic acid hydrazides with antitumor activity. *Eur. J. Med. Chem.*, 44(4) 1500-1508.
50. Atif A., Ameer S., Bendaoud A., Hsissou R., Jebbari S., Ait Sir H., and Salah M. (2025) Comprehensive evaluation of a benzimidazole-1,3,4-oxadiazole derivative for corrosion protection of C38 steel in HCl: Experimental. molecular dynamics. monte carlo. and in silico pharmacokinetic approaches. *Curr. Chem. Lett.*, 14 (4) 777-792
51. Atif A., Zahm S., Jebbari S., El Alami A., Youssoufi F., Ait Sir H., Kerraj S., and Salah. M. (2023) synthesis. admet. docking and molecular dynamics of new molecules derivatives from 1,3,4-oxadiazole and 1,3,4-bisoxadiazole: new compounds against hiv. *Eur. Chem. Bull.*, 12 (12) 4139 – 4156
52. Atif A., Marghich M., Nabil N., El Alami A., Daoudi N., Harit T., Youssoufi F., Salah M., Bitar A., and Ait Sir H. (2025) Design. synthesis. and antidiabetic evaluation of novel 1,3-di(1,3,4-oxadiazol-2-yl)benzene derivatives as potent pancreatic  $\alpha$ -amylase inhibitors: In vitro and in silico approaches. *Curr. Chem. Lett.*
53. Elhorri A. M., Belaid K. D., Zouaoui–Rabah M., and Chadli R. (2018) Theoretical study of the azo dyes dissociation by advanced oxidation using Fukui indices. DFT calculations. *Comput. Theor. Chem.*, 1130 (2018) 98-106.
54. Isravel A. D., Jeyaraj J. K., Thangasamy S., and John W. J. (2021) DFT. NBO. HOMO-LUMO. NCI. stability. Fukui function and hole–Electron analyses of tolcapon. *Comput. Theor. Chem.*, 1202 (2021) 113296-113307.
55. Cao Y., Malekshah R. E., Heidari Z., Pelalak R., Marjani A., and Shirazian S. (2021) Molecular dynamic simulations and quantum chemical calculations of adsorption process using amino-functionalized silica. *J. Mol. Liq.*, 330 (2021) 115544-115557.
56. Khaled K. F., and El-Maghraby A. (2014) Experimental. Monte Carlo and molecular dynamics simulations to investigate corrosion inhibition of mild steel in hydrochloric acid solutions. *Arab. J. Chem.*, 7 (3) 319-326.
57. Domingo L. R., Pérez P., and Sáez J. A. (2013) Understanding the local reactivity in polar organic reactions through electrophilic and nucleophilic Parr functions. *RSC Adv.*, 3 (5) 1486-1494.
58. Figueroa-Valverde L., Díaz-Cedillo F., Camacho-Luis A., López Ramos M., and Garcia Cervera E. (2010) Synthesis of a dihydrotestosterone–ciprofloxacin conjugate: relationship between descriptors log P.  $\pi$ . R m. and V m and its antibacterial activity in *S. aureus* and *E. coli*. *Monatsh. Chem.*, 141 (3) 373-380.
59. Abdolhosseini M., Zamani H., and Salehzadeh A. (2019) Synergistic antimicrobial potential of ciprofloxacin with silver nanoparticles conjugated to thiosemicarbazide against ciprofloxacin resistant *Pseudomonas aeruginosa* by attenuation of MexA-B efflux pump genes. *Biologia.* 74 (9) 1191-1196.
60. Thai, T., Salisbury, B. H., & Zito, P. M. (2025). *Ciprofloxacin*. In StatPearls. StatPearls Publishing. Retrieved October 24, 2025, from <https://www.ncbi.nlm.nih.gov/books/NBK482441/>
61. « RCSB PDB: Homepage ». Consulté le: 22 octobre 2025. [En ligne]. Disponible sur: <https://www.rcsb.org/>
62. Sharma S., Sharma A., and Gupta U. (2021) Molecular Docking studies on the Anti-fungal activity of *Allium sativum* (Garlic) against *Mucormycosis* (black fungus) by BIOVIA discovery studio visualizer 21.1. 0.0.
63. Gilad Y., Tuchinsky H., Ben-David G., Minnes R., Gancz A., Senderowitz H., Luboshits G., Firer M. A., and Gellerman. G. (2017) Discovery of potent molecular chimera (CM358) to treat human metastatic melanoma. *Eur. J. Med. Chem.*, 138 (2017) 602-615.
64. Wang Q., He J., Wu D., Wang J., Yan J., and Li H. (2015) Interaction of  $\alpha$ -cyperone with human serum albumin: Determination of the binding site by using Discovery Studio and via spectroscopic methods. *J. Lumin.*, 164 (2015) 81-85.
65. Mouhib A., Kadiri F., Yamari I., Es-Sounni B., Raji H., El Abbouchi A., El Kazzouli S., Chegdani F., El Yazidi M., Mazoir N., Chtita S., and Bakhouch M. (2025) Novel Hybrids-based quinazolinone: Synthesis. characterization. in vitro and in silico antibacterial investigations. *J. Indian Chem. Soc.*, 102 (9) 101934-101952.
66. Chen X., Chen Y., Cui J., Li Y., Liang Y., and Cao G. (2021) Molecular dynamics simulation and DFT calculation of “green” scale and corrosion inhibitor. *Comput. Mater. Sci.*, 188, 110229.
67. Ahmad Z. U., Chao B., Konggadinata M. I., Lian Q., Zappi M. E., and Gang D. D. (2018) Molecular simulation and experimental validation of resorcinol adsorption on Ordered Mesoporous Carbon (OMC). *J. Hazard. Mater.*, 354 (2018) 258-265.
68. Belghiti M. E., Bouazama S., Echih S., Mahsoun A., Elmelouky A., Dafali A., Emran K. M., Hammouti B., and Tabyaoui M. (2020) Understanding the adsorption of newly Benzylidene-aniline derivatives as a corrosion inhibitor for carbon steel in hydrochloric acid solution: Experimental. DFT and molecular dynamic simulation studies. *Arab. J. Chem.*, 13 (1) 1499-1519.
69. Shokry H. (2014) Molecular dynamics simulation and quantum chemical calculations for the adsorption of some Azo-azomethine derivatives on mild steel. *J. Mol. Struct.*, 1060 (2014) 80-87.
70. El-Hajjaji F., Messali M., Aljuhani A., Aouad M. R., Hammouti B., Belghiti M. E., Chauhan D. S., and Quraishi M. A. (2018) Pyridazinium-based ionic liquids as novel and green corrosion inhibitors of carbon steel in acid medium: electrochemical and molecular dynamics simulation studies. *J. Mol. Liq.*, 249 (2018) 997-1008.

71. Beniken M., Salim R., Ech-chihbi E., Sfaira M., Hammouti B., Touhami M. E., Mohsin M. A., and Taleb M. (2022) Adsorption behavior and corrosion inhibition mechanism of a polyacrylamide on C-steel in 0.5 M H<sub>2</sub>SO<sub>4</sub>: Electrochemical assessments and molecular dynamic simulation. *J. Mol. Liq.*, 348 (2022) 118022-118036.



© 2026 by the authors; licensee Growing Science, Canada. This is an open access article distributed under the terms and conditions of the Creative Commons Attribution (CC-BY) license (<http://creativecommons.org/licenses/by/4.0/>).